ORIGINAL RESEARCH

Regional stochastic ground-motion model for low to moderate seismicity area with variable seismotectonic: application to Peninsular India

Ketan Bajaj[1] · P. Anbazhagan[1] (ORCID)

Abstract

A new stochastic ground motion prediction equation (GMPE) for low and diverse seismicity region, i.e., Peninsular India has been derived for a wide range of magnitude (M_w 4–8) and distance (10–500 km). Source, path, and site terms have been determined by comparing the recorded and simulated response spectra using derived values from the literature. Uncertainty has been assessed through simulation by random sampling of the corresponding distribution of all the input parameters. To capture the non-uniform seismicity of Peninsular India, GMPE has been derived using constant stress and variable stress model. The synthetic data has been regressed using linear mixed-effect model algorithm by determining the functional form that is compatible for magnitude and distance scaling. Sensitivity analysis has been used in determining the impact of uncertainty of each input parameter on GMPE standard deviation. Further, new GMPEs have been validated using the recorded ground-motion data.

Keywords Peninsular India · Seismicity · GMPE · Intra plate · Crossed and nested regression

1 Introduction

Peninsular India was once considered as a stable continental region. However, the frequency of moderate earthquakes has increased in the last few decades. Significant earthquakes such as 1967, Koyna (M_w 6.3); 1993, Latur (M_w 6.1); 1997 Jabalpur (M_w 5.8); 2001 Bhuj (M_w 7.6) grab the attention of many researchers for reliable estimation of hazard values. Because of the scarcity of recorded data; till date, unresolved issues exist regarding the determination of the ground motions for specific magnitude, distance, and site condition in Peninsular India. Empirical ground motion prediction equation (GMPE) is one of

✉ P. Anbazhagan
anbazhagan@iisc.ac.in

Ketan Bajaj
ketanbajaj@iisc.ac.in

[1] Indian Institute of Science, Bangalore, India

the most preferable ways for estimating the ground motion as it can be advanced with the regional attenuation characteristics.

Many researchers have highlighted the possibility of the occurrence of earthquakes in Peninsular India (PI) because of reactivation of faults. However, till date, only one regional GMPE (Raghukanth and Iyengar 2007) is available for PI, which underpredicts the peak ground acceleration (PGA) for various regions in PI (Anbazhagan et al. 2016). Moreover, the lack of recorded ground motion data makes hazard prediction more challenging for PI. However, the advancement in the ground motion simulation algorithms and regression techniques help in resolving this issue theoretically. A significant challenge in the simulation of the ground motion is the proper calibration of its variability that can be reflected by the variation of the simulation. It is resolved by studying the impact of the distribution of the stochastic model's inputs resulting in between-event and within-event ground motion variability.

The present study aims at developing a robust GMPE for Peninsular India by varying the seismotectonic parameters. The synthetic ground motion data has been generated using the Finite-Fault stochastic model (EXSIM) developed by Motazedian and Atkinson (2005) and improved by Boore (2009). The recorded and simulated response spectra have been compared to determine the site-dependent source and site parameters, i.e., stress drop, anelastic attenuation, kappa, and corner frequency for PI. The simulation of PGA and spectral acceleration (0.01–10 s) has been performed for a wide range of moment magnitude (4–8) and hypocentral distance (10–500 km) for standard rock condition having V_{S30} of 2000 m/s. Considering the diverse seismicity of PI, variable and constant stress GMPE models have been used for capturing the ground motion variability in PI. The functional form that represents the magnitude and hypocentral distance scaling have been selected based on the mixed effect analysis approach. The simulated ground motion has been regressed using linear mixed effect approach. Further, all the input parameters have been considered as random variables, and the uncertainty in the simulation have been accomplished through random sampling of the input parameters distribution. Sensitivity analysis has been used to assess the impact of the uncertainty of each input parameter on the final GMPE uncertainty. Finally, the new GMPEs have been tested with the available recorded strong motion data.

2 Geology, seismicity, and seismotectonic of Peninsular India

Peninsular India is referred as one of the oldest geological formation landmass and tectonically stable continental crust. The geological provision of Southern India, part of the study area, is shown in Fig. 1. Majorly, PI is classified as Gneissic complex/Gneissic granulite with primary inoculation of greenstone and allied supracrustal belt. The geological feature of PI is the union of various crustal terranes that were assembled due to geodynamic processes running from mid-Archean to Neo-Proterozoic time and a few sedimentary basins. Tectonically and geologically PI can be majorly divided into Deccan Volcanic Province (DVP), Dharwar craton (DC), South Granulite Terrain (SGT), Cuddapah basin (CB), Bastar Craton and Eastern and the Western Ghats. DC is one of the most prominent cratons of PI and considering to the metamorphism, lithologies, and formation ages; it is further classified as, Eastern Dharwar Craton (EDC) and Western Dharwar Craton (WDC) (See Fig. 1). The eastern portion of EDC is resided by the Cuddapah Basin, which is a sedimentary basin and comprises of igneous and sedimentary
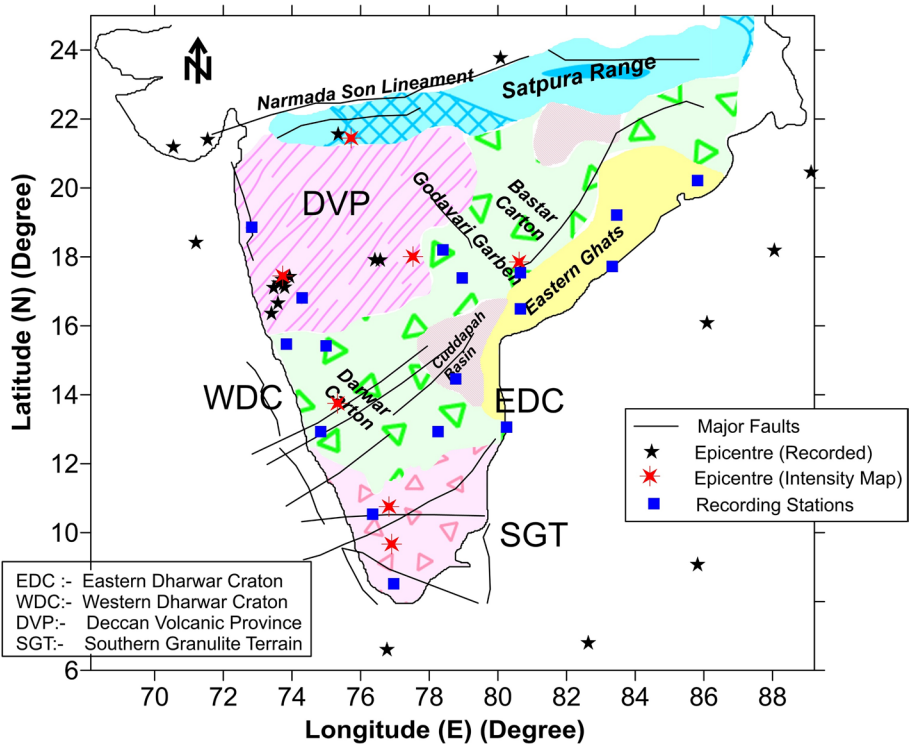
Fig. 1 Geological structure, major faults and significant earthquakes in Peninsular India

rocks of the Cuddapah and Kurnool Groups. The southern part of PI consists of Archean metamorphic terrain (2.6 Ga), called as the SGT, comprising of polydeformed Archaean and Proterozoic high-grade metamorphic and magmatic rocks (Meert et al. 2010). DVP covers the large part of PI and result of stupendous outburst of volcanic energy. DVP overlies the Precambrian basement of cratons and mobile belt of Indian shield of several layers with variable thickness (Subbarao and Hooper 1988).

Seismotectonic of PI has been permeated because of the occurrence of nonuniform micro-seismicity belts from the faults developed due to the amalgamation of various geological blocks. Being a stable continental region, PI has irregular seismicity. For example, microseismicity has been observed near to SGT, whereas, EDC has moderate seismicity. Rao (2000) concluded the increase in heat flow rifts like Godavari, Damodar-Mahanadi, Aravali and Saurashtra-Narmada-Son lineament which is a reliable indicator of increasing intraplate deformation in the lithosphere of PI (See Fig. 1). A nonuniform thickness below the Peninsular Indian Shield indicated juxtaposition of cratonic blocks of discrete thickness, geology rifts, and faults and resulted in the accumulation of stress and release of strain energy in the form of microearthquakes (Gupta and Kumar 2002). PI is also covered by various faults, ridges, shear zones and tectonic lineaments. Rastogi (1992) indicated the NW–SE, NE–SW, NNW–SSE, and WNW–ESE trending sets of faults in PI. Various researches (Gupta 2006; Ramaswamy 2006; John and Rajendran 2008 etc.) presented and mapped the active tectonic feature (lineaments and faults) in

PI. In addition to land faults, PI is also surrounded by diverse and complex tectonics features along the Indian ocean (Murthy et al. 2011).

3 Database used

The available recorded ground motion for PI is taken from the Indian seismic and GNSS network (ISGN) and different published literature. The available instrumental ground motion data consists of 21 recorded moderate earthquakes occurred in PI. Out of 21, 17 recorded earthquakes from 2010 to 2018 are taken from ISGN with M_w of 4.0–5.2 and a hypocentral distance (R) between 30 and 500 km (Fig. 1). In total, 85 recorded ground motions are available, out of which 52 have been used in the study and remaining are ignored because of poor signal to noise ratio (Fig. 1). The obtained database has been baseline corrected, instrument corrected, and band-pass filtered between 0.25–0.9 Hz and 25–27 Hz. Further, three earthquakes near to Koyna-Warna region is taken from Gupta and Rambabu (1993). Additionally, the aftershock of 1993 Killari earthquake is obtained from Baumbach et al. (1994). The two ground motions of 1997 Jabalpur earthquake are collected from Singh et al. (1999). The detail of these five earthquakes is also available in Iyengar and Raghu Kanth (2004). Most of the instrument data is available only after 1980 (Anbazhagan et al. 2015). Before that only isoseismal maps are available. Isoseismal maps from seven earthquakes, i.e., 1990 Coimbatore (6.3 M_w); 1967 Koyna (6.5 M_w); 1993 Killari (6.1 M_w); 1938 Satpura (6.3 M_w); 1969 Bhadrachalam (5.7 M_w); 2000 Pala (4.7 M_w); and 1975 Shimoga (4.7 M_w) have also been used. Details of these Isoseismal maps are given in Anbazhagan et al. (2013). Modified Mercalli Intensity (MMI) has been converted to PGA using MMI-PGA relation proposed by Nath and Thingbaijam (2012). As, this is the only equation available for region and used in the study with inherent uncertainty. Total 21 recorded and 7 non-instrumental earthquakes are further used in determining the seismological parameters for simulating the synthetic ground motions. The detail of these earthquakes is given as Table 5 (appendix). The database does not have instrumental data for the entire range of magnitude and distance; hence it cannot be used for empirical ground motion.

4 Simulation parameters

The simulated time histories obtained from the algorithm proposed by Motazedian and Atkinson (2005) is based on a given set of parameters, which varies from site to site. For simulating a large number of ground motions, these model parameters need to be defined, so that variability in a GMPE can be captured. To account these variabilities; stress model, duration model, attenuation model and focal depth have been estimated based on the recorded waveform in Peninsular Shield of India.

4.1 Stress drop

The dependency of stress drop on magnitude size is still debatable. Researchers (e.g. Ide et al. 2003) concluded dependency of stress drop ($\Delta\sigma$) on size of the earthquake. However, few studies (e.g. Allmann and Shearer 2009) highlighted that for large earthquakes; stress drop remains constant. Considering locally recorded earthquakes near to Koyna Dam,

Gupta and Rambabu ([1993](#)) derived the source parameter for earthquake size varying from 3.2 to 6.5. Using the same algorithm, Yadav et al. ([2013](#)) calculated the stress drop for 38 local earthquakes near to Koyna-Warna region. In this study, stress drop is also calculated for earthquakes recorded in Maharashtra and Karnakata–Maharashtra boundary. Considering the previously and recently derived stress drop, a new relationship between stress drop and magnitude has been derived for PI. Figure [2](#)a shows the variation between the stress drop and moment magnitude. The relation between $\Delta\sigma$ and M_w is given as

$$\log(\Delta\sigma) = 0.358M_w + 0.551 \tag{1}$$

As 6.5 (Koyna Earthquake) is the maximum recorded earthquake in PI, however, the ground motion data is simulated till M_w 8. Hence, similar to Darragh et al. ([2015](#)), for $M_w > 6.5$, the above equation is extrapolated till 8 M_w and stress drop is determined.

Singh et al. ([1999](#)) concluded the stress drop variation of 100 to 300 bars for Peninsular Indian shield, which was further used by Raghukanth and Iyengar ([2007](#)). Allmann and Shearer ([2009](#)) suggested that for the larger magnitudes, stress drop remains constant, a similar assumption was considered by Drouet and Cotton ([2015](#)). Furthermore, the approximate mean value of variation of stress drop of 30 bars and 60 bars for interplate and intraplate region respectively was reported by Allmann and Shearer ([2009](#)). Bajaj and Anbazhagan ([2018a](#)) calculated the stress drop for the Himalayan region and concluded a constant stress drop of 50, 100 and 150 bars for M_w more than 5.5. However, in this study, for the constant stress drop model, the mean variation of stress drop at different magnitudes has been found (See Fig. [2](#)b). A jump of approximate of factor two in stress drop has been observed for M_w greater than 5.5. Hence, the resulting constant average stress drop of 150 bars is considered for M_w less than 5.5 and 300 bars for M_w more than 5.5. Magnitude-dependent stress drop value uncertainty varies from 0.2 for large events and 0.5 for smaller events on $\log_{10}$ scale. Hence in this study, both dependency and independency of stress drop on magnitude is considered for simulating ground motions.

4.2 Attenuation and duration

The attenuation parameter has been divided into two parts, one being geometric spreading and other being anelastic attenuation. Former is a predominant scattering of energy
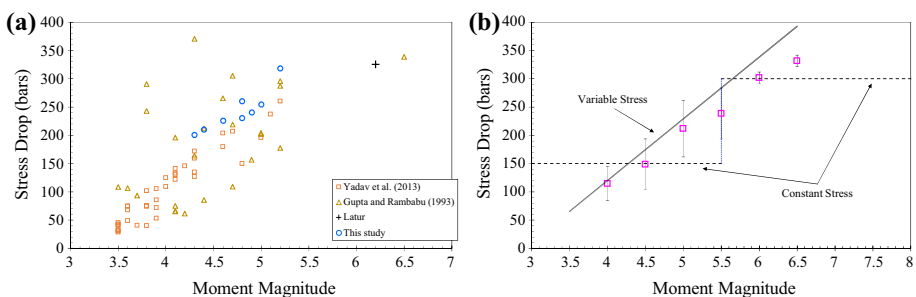

Fig. 2 **a** Inverted stress drop versus moment magnitude from the present and previous study for different parts of Peninsular India and **b** model stress parameter used for simulating the ground motion using variable and constant stress model. Open square represents the average stress at a particular magnitude along with standard deviation

because of small-scale heterogeneities, discontinuities, and fractures, and the latter is a predominant dissipation of energy in micro-cracks, joints of the rock masses, and partial melts (Frankel and Wennerberg 1987). Due to the lack of the near-field data, these attenuation factors have not been derived in this study, instead considered from the published literature.

Based on the far-field data, Singh et al. (1999) defined the geometric spreading parameter for PI Shield. Both linear and bilinear functional form of geometric attenuation have been tested considering the recorded data of PI Shield near Maharashtra, Hyderabad, and Vishakhapatnam with $4.8 \leq M_w \leq 6.0$. The response spectra of the recorded and simulated ground motion data have been compared. Response spectra simulated from bilinear function form is giving a better result than linear one for EDC, WDC, and SGT. However, a linear function is giving better result in case of DVP and Koyna. The detail regarding the form of geometric attenuation used for different regions is given as Table 1. Similarly using the same methodology, kappa factor (κ) has been derived. The derived κ is 0.006 ± 0.001 s for all the five regions for PI.

Very few studies are present to determine the anelastic attenuation for PI. Kumar et al. (2007) considered the broadband stations at Dharwar, Cuddapah, and Kothagudem regions and determined anelastic attenuation as $Q_c = 730.62f^{0.54}$, $Q_c = 535.06f^{0.59}$, and $Q_c = 150.56f^{0.91}$ respectively. Singh et al. (2012) determined Q_c at different parts of Peninsular India. Recently, Sivaram et al. (2017) presented the Q_c value at different parts of Peninsular India by dividing it into EDC, WDC and SGT. Q_c value was calculated for EDC, WDC and SGT as $Q_c = 664f^{0.47}$, $Q_c = 1165f^{0.44}$ and $Q_c = 568f^{0.67}$ respectively. As explained above, simulations have been done by dividing the whole Peninsular India into five parts. Hence, $Q_c = 664 \pm 8f^{0.47 \pm 0.01}$, $Q_c = 1165 \pm 14f^{0.44 \pm 0.01}$, $Q_c = 568 \pm 6f^{0.67 \pm 0.01}$, $Q_c = 455 \pm 30f^{0.69 \pm 0.05}$ and $Q_c = 117 \pm 2f^{0.97 \pm 0.07}$ are used for EDC, WDC, SGT, DVP and Koyna region respectively.

Another important parameter in the simulation of ground motion is the path duration function. The total duration (T_d) is the combination of the source duration (T_s) which is assumed to be the reciprocal of corner frequency (Boore 2003) and path duration (T_p) which relates to propagation effects and the other effects linked with the site condition and complex source effect. Due to lack of recorded data, it is difficult to derive a new duration model. Hence, in this study, duration model derived by Anbazhagan et al. (2017) has been used for simulating the ground motion, as it includes PI recorded data also. The simulation parameters have been used in the present study are given in Table 1 by dividing the whole Peninsular Indian shield into five different parts as EDC, WDC, SGT, DVP and Koyna region.

5 Data simulation for Peninsular India

For deriving a new GMPE for Peninsular India, ground motion were simulated for EDC, WDC, SGT, DVP, and Koyna separately by considering both variable and constant stress drop. Simulations have been performed for moment magnitude range of 4–8, using 0.1-unit step and distance range of 5–500 km. For each earthquake, a random fault orientation has been defined, i.e., strike and dip. Similar to Drouet and Cotton (2015), a fictitious fault mechanism has been assigned based on the dip angle, i.e., for reverse mechanism a dip lower than 40°, for strike-slip mechanism dip greater than 75° and normal mechanism

Table 1 Parameters used for simulating the synthetic ground motion

Parameter	Distribution	Mean					SD
		EDC	WDC	SGT	DVP	Koyna	
Magnitude (M_w)	–	4–8	4–8	4–8	4–8	4–8	–
Hypocentral distance (km)	–	5-500	5-500	5-500	5-500	5-500	–
Fault length and width (km)	Normal	Blaser et al. (2010)					0.3
Shear wave velocity (km/s)	–	3.5					–
Crustal density (g/cm²)	–	2.8					–
Stress drop (bars)	Log-normal	Variable stress		$\log(\Delta\sigma) = 0.358 M_w + 0.551$			0.2 for $M_w \leq 5.5$ and 0.5 for $M_w > 5.5$
	–	Constant stress		150 bars for $M_w \leq 5.5$ and 300 bars for $M_w > 5.5$			
Geometric spreading	Normal	$G = \begin{cases} R^{-1}, & R \leq R_x \\ (RR_x)^{-1/2}, & R > R_x \end{cases}$, $\quad R_x = 100$		$G = R^{-1/2}, \quad$ for all R			10 in case of R_x
Anelastic attenuation	Normal	$Q_c = 664 \pm 8 f^{0.47 \pm 0.01}$	$Q_c = 1165 \pm 14 f^{0.44 \pm 0.01}$	$Q_c = 568 \pm 6 f^{0.67 \pm 0.01}$	$Q_c = 455 \pm 30 f^{0.69 \pm 0.05}$	$Q_c = 117 \pm 2 f^{0.97 \pm 0.07}$	8–30 in Q_0 and 0.01–0.07 in n
Duration	Normal	Anbazhagan et al. (2017)					6.5
κ (s)	Normal	0.006					0.001

otherwise. For the various distance metrics, the uniform distribution of the dip angle has been assumed because of the following two reasons (1) focal mechanism is not included as predictor variable and (2) fault orientation is only used for calculating the fault dimensions.

Another significant factor in the synthetic simulation of ground motions is the hypocentral depth. Depth was estimated based on the updated catalog of earthquake events for entire Peninsular India. For EDC, WDC, SGT, DVP and Koyna, the reported range of hypocentral depth respectively is 10–90 km, 5–60 km, 5–33 km, 5–150 km and 10–60 km (CMT Harvard and USGS). Reported average hypocentral depth for the entire PI is 35 km. Hence, for simulating the ground motion data, hypocentral depth has been considered as a normal distribution with mean and standard deviation as 35 ± 10 km.

Relationships derived by Blaser et al. (2010) have been used for determining the fault dimensions (rupture length and rupture width). Blaser et al. (2010) developed the empirical relationship between rupture length and M_w, and rupture width and M_w for different fault orientation. For a particular magnitude, rupture length and width have been determined using Blaser et al. (2010) equations. To include variability in the fault dimensions, the mean rupture length, and width and standard deviation (from Blaser et al. 2010 equations) have been used to generate samples using normal distribution. This allows for simulating fault planes of different dimensions for same magnitude. The relationships derived by Blaser et al. (2010) are valid for $M_w > 4.8$, therefore, these equations have been extrapolated beyond the validity range, especially for small magnitudes (Drouet and Cotton 2015). The extrapolation does not have strong influence on the simulation due to having the small extension in case of small magnitude. This is only used to compute the different distance matrices. Fifty different mechanisms have been simulated for each moment magnitude with magnitude bin size 0.1 M_w.

Using the given focal mechanism and magnitude (M_w 4–8), epicentral distance from 10 to 500 km and from source-to-site azimuths from 0° to 360° have been simulated. The maximum epicentral distance has been selected as 500 km by studying the damage distribution map of the pre-instrumented earthquake (1900 Coimbatore, 1967 Koyna, 1993 Killari earthquake). The concept of apparent station (AS) has been used for simulating each event at different hypocentral distance (Anbazhagan et al. 2013). The AS is established at 50 locations with azimuths covering the range of 0°–360° around the epicenter with azimuth bin size of 7.2°. Hence, every next AS is at a distance of 10 km with an azimuth difference of 7.2° from the successive stations. AS concept is useful in determining the SA in both forward and backward direction of fault.

Figure 3 shows the simulated spectral acceleration at zero period for EDC, WDC, SGT, DVP and Koyna regions versus hypocentral distances and for M_w 4.7 and M_w 6.5 (1967, Koyna earthquake), considering variable stress model and standard rock condition. The medians of GMPEs of NGA-East project, previously developed PI GMPEs and recorded PGA values are compared with the simulated data. Simulated and the recorded data are not consistent with the predictive equation developed for stable continental region (See Fig. 3). For higher magnitude and distance less than 150 km, a significant difference is observed in ground motion data. One of the reasons may be that the GMPEs developed under the NGA-East project do not consider the Indian recorded data. For significant earthquake instead of recorded data, isoseismal maps are available. Similar to Singh et al. (1999), MMI has been converted into PGA and used for comparing the simulated data. Regression equation developed by Nath and Thingbaijam (2012) is used for this purpose. It can be also noted from Fig. 3 that there is no significant difference in the simulated data is observed for all the five regions in case of variable stress model. Similar observation has been drawn in case of the constant stress model. In comparison, it has been also observed that at large distances and
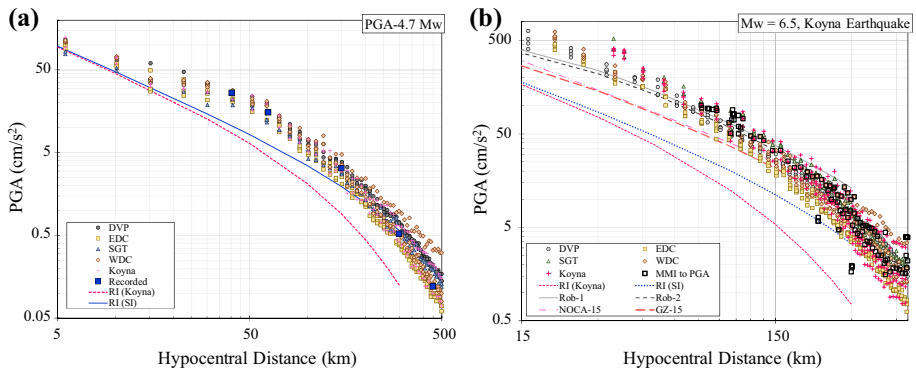
Fig. 3 Stochastically simulated spectral acceleration at zero periods for Eastern Dharwar Craton (EDC), Western Dharwar Craton (WDC), South Granulite Terrain (SGT), Deccan Volcanic Province (DVP) and Koyna region considering variable stress model. Simulated data has shown for **a** 4.7 M_w and **b** 6.5 M_w (Koyna Earthquake). Simulated data is compared with the recorded PGA and PGA converted from Intensity

higher magnitude the difference in the spectral acceleration values is significant using of variable and constant stress model. This has been taken care by while selecting the functional form of the GMPE further. For 1967 Koyna earthquake, simulated data has been compared with the MMI-PGA and compared with the Raghukanth and Iyengar (2007), Darragh et al. (2015), Grazier (2015) and Al Noman and Cramer (2015). Raghukanth and Iyengar (2007), Darragh et al. (2015), Grazier (2015) and Al Noman and Cramer (2015) is referred as RI, Rob, GZ-15, and NOCA-15 in Fig. 3.

6 Selection of functional form and regression analysis

With the improvement in the recording database and upgrading of simulation algorithms, new GMPEs are being compounded with various parameters in its functional form. However, a basic functional form of a GMPE should account for magnitude dependence and saturation along with attenuation of stress waves with distance due to spreading and material damping. In this study, algorithm proposed by Bajaj and Anbazhagan (2018b) is used for selecting the functional form for Peninsular India. More details regarding various functional form available and methods for selecting are presented in Bajaj and Anbazhagan (2018b).

As explained above, PI lacks in recorded ground motion, but reasonable Isoseismal maps are available. Hence for selecting a particular functional form, Nath and Thingbaijam (2012) regression equation has been used for converting intensity into PGA. It can be noted here that this is the only conversion relation available for PI and there may be inherent uncertainty in the converted values. Seven functional forms considered by various researchers for the stable continental region have been used in this study. These functional forms are given as Table 2. Magnitude scaling was accounted using both quadratic and bilinear functional form. Equation 3 is having non-linear quadratic function for M ≤ 6 and linear for M > 6. To account for the distance scaling, simple functional form comprising product of a linear function of magnitude and the logarithm of distance was used. The linear term explains the decrease in attenuation with an increase in magnitude size. However, EQ4 and EQ5 describe the calibration of distances at various points to account the

Table 2 Functional form used to consider magnitude and distance scaling

Sl. no.	Abbreviation	M-scaling	R-scaling	Bias value	σ
1	EQ1	$c_1 + c_2 M + c_3 M^2$	$(c_4 + c_5 M)\ln R + c_6 R$	0.235	0.627
2	EQ2	$c_1 + c_2(M-6) + c_3(M-6)^2$	$c_4 \ln R + c_5 R$	0.258	0.687
3	EQ3	$\begin{cases} c_1 + c_2(M-6) + c_3(M-6)^2 \\ c_1 + c_4(M-6) \end{cases}$	$(c_5 + c_6 M)\ln R + c_7 R$	0.095	0.424
4	EQ4	$c_1 + c_2 M + c_3 M^2$	$(c_4 + c_5 M) * \min(\ln R, \ln(60)) + (c_6 + c_7 M) * \max\left(\min\left(\ln\left(\frac{R}{60}\right), \ln\left(\frac{120}{60}\right)\right), 0\right)$ $+ (c_8 + c_9 M) * \max\left(\ln\left(\frac{R}{140}\right), 0\right) + c_{10} R$	0.157	0.534
5	EQ5	$c_1 + c_2(M-6) + c_3(M-6)^2$	$(c_4 + c_5 M) * \min(\ln R, \ln(60)) + (c_6 + c_7 M) * \max\left(\min\left(\ln\left(\frac{R}{60}\right), \ln\left(\frac{120}{60}\right)\right), 0\right)$ $+ (c_8 + c_9 M) * \max\left(\ln\left(\frac{R}{140}\right), 0\right) + c_{10} R$	0.189	0.567
6	EQ6	$c_1 + c_2(M-6) + c_3(M-6)^2$	$(c_4 + c_5 M)\ln R + c_6 R$	0.204	0.615
7	EQ7	$\begin{cases} c_1 + c_2(M-6) + c_3(M-6)^2 \\ c_1 + c_4(M-6) \end{cases}$	$(c_5 + c_6 M) * \min(\ln R, \ln(60)) + (c_7 + c_8 M) * \max\left(\min\left(\ln\left(\frac{R}{60}\right), \ln\left(\frac{120}{60}\right)\right), 0\right)$ $+ (c_9 + c_{10} M) * \max\left(\ln\left(\frac{R}{140}\right), 0\right) + c_{11} R$	0.135	0.521

scattering of waves at different distances. This functional form is considered by Pezeshk et al. (2015, 2018) for deriving GMPE for Central and Eastern North America.

For determining the best functional form out of seven (See Table 2), Isoseismal maps from five earthquakes, i.e., 1990 Coimbatore (M_w 6.0); 1967 Koyna (M_w 6.5); 1993 Killari (M_w 6.1); 1969 Bhadrachalam (M_w 5.7); and Shimoga (M_w 4.7) have been used. Details of these Isoseismal maps can be referred from Anbazhagan et al. (2013). Considering the simulated data, coefficients for PGA have been derived for all the seven functional forms of GMPE. Residual has been calculated from the predicted PGA (using GMPEs) and recorded PGA (converted from intensity) value using Eq. 2.

$$(R_{i,j})_k = \ln\left(SA_{i,j}\right)_{data} - \ln\left(SA_{i,j}\right)_k \tag{2}$$

Index i, j and k, respectively, refers to the earthquake event, recording within the event i and a particular GMPE functional form given in Table 2. Further, using mixed effect analysis on residuals; bias, intraevent residual and interevent residual for all the functional forms has been calculated using Eq. 3.

$$(R_{i,j})_k = c_k + \left(\eta_i\right)_k + \left(\epsilon_{i,j}\right)_k \tag{3}$$

where c_k is the mean offset (or bias) of the data relative to GMPE functional form k, η_i represents the event term for event i and $\epsilon_{i,j}$ is the intraevent residuals for recording j in event i. The event term η_i represents the mean offset of data for event i from the prediction provided by the GMPE median after adjusting the offset c_k. In other words, the intraevent residual $\epsilon_{i,j}$ is the residual after accounting for the interevent residual η_i. Interevent (η) and Intraevent (ϵ) terms are assumed to have zero mean and τ and ϕ respectively as standard deviation. Hence, τ refers to the event-to-event variability and on the other hand, ϕ refers to the variability in a single event.

Using that total standard deviation (σ) has been calculated considering the square root of sum of square of standard deviation from intraevent and interevent residual i.e. $\sigma = \sqrt{\tau^2 + \phi^2}$. Details about the calculations and algorithm can also be referred from Bajaj and Anbazhagan (2018b) and Skarlatoudis (2017). The average bias and σ calculated from all the five earthquakes for all the seven GMPE functional form is given as Table 2. Equation 3 shows the least average bias value and σ value. Hence, EQ3 is further used for deriving the new GMPE for Peninsular India considering variable and constant stress drop.

The GMPEs functional form given below has been used for deriving the coefficients at different spectral periods considering variable and constant stress drop

$$\ln Y = \begin{cases} c_1 + c_2(M-6) + c_3(M-6)^2 + \left(c_5 + c_6 M\right)\ln R + c_7 R + \epsilon\sigma & M \leq 6 \\ c_1 + c_4(M-6) + \left(c_5 + c_6 M\right)\ln R + c_7 R + \epsilon\sigma & M > 6 \end{cases} \tag{4}$$

where $\ln Y, M, R, \epsilon$, and σ are respectively logarithm of ground motion, magnitude, hypocentral distance, standard normal variable and standard deviation and $c_1, c_2, c_3, c_4, c_5, c_6$ and c_7 are the corresponding regression coefficients. For determining the regression coefficients for a new GMPE, *lme4* R package in Bates et al. (2013) has been used (Stafford 2014). The regression coefficients corresponding to $c_1, c_2, c_3, c_4, c_5, c_6$ and c_7 for different periods considering variable and constant stress drop are given in Tables 3 and 4 respectively. The calculated PGA and PSA values are in "g". The correlation coefficient for the different periods vary from 0.85 to 0.93.

Figure 4 shows the comparison between variable and constant stress models for a standard rock condition for all magnitudes and distance for PI. For the large magnitude and less distance, the variation in the models is significant (See Fig. 4). However, for smaller

Table 3 Regression coefficients for PGA and PSA at different period along with confidence interval calculated using Monte Carlo Simulation for variable stress model

T (s)	c_1	c_2	c_3	c_4	c_5	c_6	c_7	τ	Φ	σ
PGA	2.955 ± 0.12	0.589 ± 0.02	− 0.216 ± 0.05	0.486 ± 0.01	− 1.878 ± 0.01	0.098 ± 0.002	− 0.005 ± 0.0001	0.373	0.553	0.667
0.01	2.986 ± 0.12	0.481 ± 0.02	− 0.226 ± 0.05	0.459 ± 0.01	− 1.974 ± 0.02	0.113 ± 0.002	− 0.005 ± 0.0001	0.379	0.575	0.689
0.02	2.874 ± 0.12	0.477 ± 0.02	− 0.214 ± 0.05	0.466 ± 0.01	− 1.829 ± 0.02	0.102 ± 0.002	− 0.005 ± 0.0001	0.384	0.603	0.715
0.03	3.129 ± 0.11	0.495 ± 0.02	− 0.208 ± 0.07	0.484 ± 0.02	− 1.822 ± 0.02	0.098 ± 0.002	− 0.005 ± 0.0001	0.391	0.629	0.741
0.04	3.270 ± 0.10	0.507 ± 0.02	− 0.206 ± 0.07	0.506 ± 0.01	− 1.801 ± 0.02	0.095 ± 0.002	− 0.005 ± 0.0001	0.398	0.650	0.762
0.05	3.403 ± 0.10	0.543 ± 0.02	− 0.202 ± 0.07	0.544 ± 0.02	− 1.768 ± 0.02	0.091 ± 0.002	− 0.005 ± 0.0001	0.402	0.665	0.777
0.06	3.407 ± 0.11	0.562 ± 0.02	− 0.216 ± 0.07	0.575 ± 0.02	− 1.691 ± 0.02	0.082 ± 0.002	− 0.005 ± 0.0001	0.405	0.664	0.778
0.1	3.308 ± 0.12	0.559 ± 0.02	− 0.244 ± 0.07	0.581 ± 0.02	− 1.681 ± 0.01	0.081 ± 0.002	− 0.005 ± 0.0001	0.399	0.634	0.749
0.15	3.103 ± 0.13	0.571 ± 0.02	− 0.278 ± 0.05	0.587 ± 0.02	− 1.653 ± 0.02	0.080 ± 0.002	− 0.005 ± 0.0001	0.382	0.557	0.675
0.25	2.748 ± 0.13	0.694 ± 0.02	− 0.324 ± 0.05	0.633 ± 0.02	− 1.592 ± 0.02	0.074 ± 0.002	− 0.004 ± 0.0001	0.375	0.517	0.639
0.5	2.046 ± 0.14	0.851 ± 0.02	− 0.371 ± 0.05	0.654 ± 0.02	− 1.558 ± 0.02	0.075 ± 0.002	− 0.004 ± 0.0001	0.373	0.500	0.624
1	0.817 ± 0.14	1.190 ± 0.02	− 0.436 ± 0.05	0.787 ± 0.03	− 1.391 ± 0.02	0.064 ± 0.002	− 0.003 ± 0.0001	0.369	0.486	0.610
2.5	− 0.542 ± 0.13	2.060 ± 0.02	− 0.067 ± 0.05	0.660 ± 0.03	− 1.910 ± 0.02	0.144 ± 0.002	− 0.002 ± 0.0001	0.355	0.478	0.595
5	− 1.890 ± 0.13	2.050 ± 0.02	0.057 ± 0.06	0.810 ± 0.02	− 2.335 ± 0.02	0.206 ± 0.002	− 0.001 ± 0.0001	0.351	0.476	0.591
7.5	− 2.837 ± 0.13	1.873 ± 0.03	0.076 ± 0.05	0.926 ± 0.03	− 2.528 ± 0.03	0.238 ± 0.002	− 0.001 ± 0.0001	0.346	0.474	0.587
10	− 3.402 ± 0.13	1.720 ± 0.03	0.073 ± 0.07	0.965 ± 0.02	− 2.675 ± 0.03	0.261 ± 0.002	− 0.001 ± 0.0001	0.323	0.453	0.556

Table 4 Regression coefficients for PGA and PSA at different period along with confidence interval calculated using Monte Carlo Simulation for constant stress model

| T (s)	c_1	c_2	c_3	c_4	c_5	c_6	c_7	τ	Φ	σ
PGA	2.642 ± 0.19	0.253 ± 0.07	-0.079 ± 0.03	-0.054 ± 0.04	-2.199 ± 0.05	0.155 ± 0.03	-0.004 ± 0.0002	0.251	0.339	0.422
0.01	2.585 ± 0.17	0.325 ± 0.09	0.0001 ± 0.00	0.003 ± 0.01	-2.149 ± 0.08	0.151 ± 0.02	-0.004 ± 0.0001	0.239	0.352	0.426
0.02	2.749 ± 0.17	0.376 ± 0.09	0.019 ± 0.02	0.058 ± 0.05	-2.091 ± 0.07	0.141 ± 0.01	-0.004 ± 0.0001	0.242	0.369	0.441
0.03	2.883 ± 0.16	0.426 ± 0.09	0.044 ± 0.02	0.103 ± 0.05	-2.042 ± 0.09	0.133 ± 0.05	-0.005 ± 0.0001	0.252	0.384	0.460
0.04	3.028 ± 0.15	0.450 ± 0.09	0.053 ± 0.02	0.111 ± 0.05	-2.020 ± 0.09	0.130 ± 0.05	-0.005 ± 0.0002	0.258	0.397	0.473
0.05	3.117 ± 0.16	0.506 ± 0.09	0.054 ± 0.02	0.159 ± 0.02	-1.945 ± 0.08	0.120 ± 0.06	-0.005 ± 0.0002	0.267	0.405	0.485
0.06	3.051 ± 0.16	0.481 ± 0.09	0.034 ± 0.02	0.150 ± 0.06	-1.913 ± 0.09	0.120 ± 0.08	-0.005 ± 0.0001	0.291	0.405	0.499
0.1	3.004 ± 0.18	0.481 ± 0.09	-0.002 ± 0.02	0.178 ± 0.09	-1.902 ± 0.09	0.118 ± 0.05	-0.004 ± 0.0002	0.319	0.402	0.513
0.15	2.729 ± 0.18	0.509 ± 0.11	-0.071 ± 0.02	0.204 ± 0.09	-1.863 ± 0.09	0.116 ± 0.03	-0.004 ± 0.0002	0.268	0.389	0.472
0.25	2.167 ± 0.19	0.619 ± 0.11	-0.159 ± 0.02	0.291 ± 0.09	-1.758 ± 0.10	0.108 ± 0.08	-0.004 ± 0.0002	0.247	0.374	0.448
0.5	1.308 ± 0.19	0.830 ± 0.10	-0.183 ± 0.03	0.346 ± 0.08	-1.808 ± 0.09	0.123 ± 0.03	-0.003 ± 0.0001	0.227	0.359	0.425
1	0.313 ± 0.20	1.102 ± 0.10	-0.161 ± 0.03	0.478 ± 0.08	-1.918 ± 0.09	0.142 ± 0.02	-0.003 ± 0.0001	0.216	0.346	0.408
2.5	-1.583 ± 0.21	1.702 ± 0.09	-0.069 ± 0.02	0.547 ± 0.07	-1.993 ± 0.08	0.173 ± 0.02	-0.002 ± 0.0001	0.209	0.337	0.397
5	-2.852 ± 0.20	1.755 ± 0.09	0.037 ± 0.02	0.772 ± 0.08	-2.432 ± 0.08	0.228 ± 0.02	-0.001 ± 0.0001	0.205	0.330	0.388
7.5	-3.962 ± 0.19	1.697 ± 0.09	0.072 ± 0.02	1.072 ± 0.08	-2.416 ± 0.08	0.226 ± 0.02	-0.001 ± 0.0001	0.202	0.324	0.382
10	-4.962 ± 0.19	1.636 ± 0.09	0.117 ± 0.02	1.123 ± 0.07	-2.596 ± 0.08	0.259 ± 0.02	-0.001 ± 0.0001	0.200	0.320	0.377
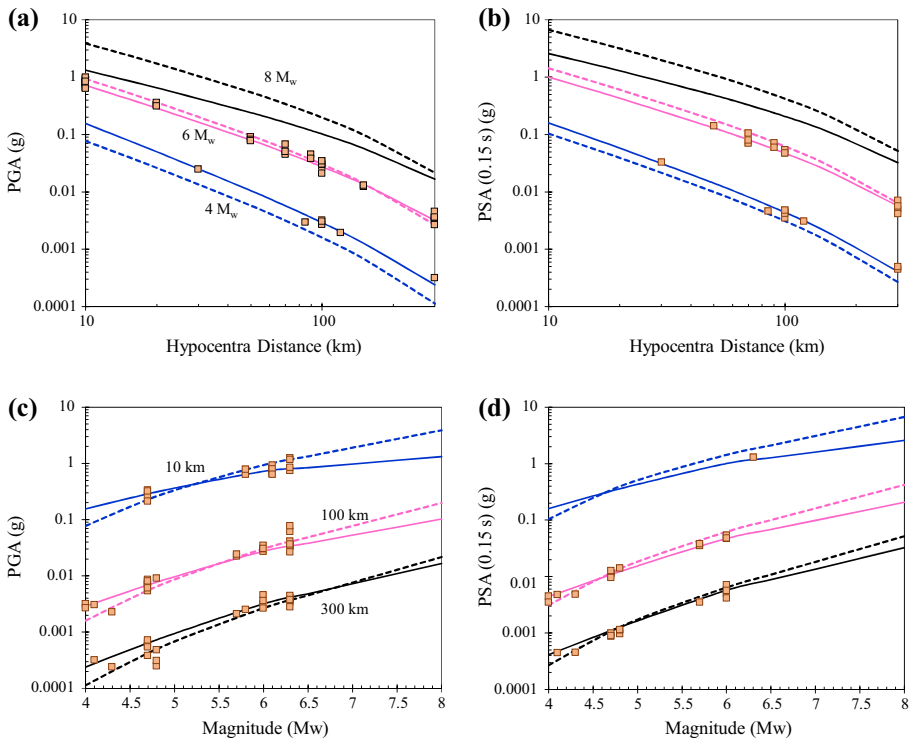
Fig. 4 Comparison of different version of stochastic GMPE, amplitude versus distance at **a** PGA and **b** PSA at 0.15 s and amplitude versus magnitude, **c** PGA and **d** PSA at 0.15 s. The dashed and solid line respectively represents the constant and variable stress. The solid rectangle represents corresponding recorded data

magnitudes and at a short hypocentral distance, the constant stress parameter leads to a higher value as compared to variable stress model. This is to be expected from the input stress parameter model. The differences are more pronounced for shorter periods as compared to longer periods. The PGA and PSA (0.15 s) values estimated from a new GMPE for different stress model are also compared with the recorded data and PGA converted using Isoseismal maps. It can be observed that the recorded data is matching well with the constant and variable stress model. The confidence interval for the respective period corresponding to each regression coefficient is given in Tables 3 and 4.

7 Sensitivity analysis and validation of gmpe

Developed GMPEs are based on the simulated ground motions data, which is highly influenced by the uncertainties in some of the input parameters. All these input parameters are governed by a particular distribution and uncertainties in these parameters are proliferated through the random sampling of the distributions. Hence, sensitivity analysis has been performed to test how these uncertainties influence the final GMPE uncertainty and how robustly the present GMPE models result in the presence of uncertainty. Set of 7

GMPEs have computed, considering; the uncertainty on each parameter, one by one (all others are set to their median values). The considered uncertainties parameters are; focal depth uncertainty, uncertainty on duration, fault plane (random orientation and hypocentral position), anelastic attenuation, geometric spreading, kappa factor and stress drop. Based on the analysis, it is seen that the coefficients determined by varying these parameters are almost identical and within the confidence interval as mentioned in Tables 3 and 4. However, the standard deviation varies a lot with the change in each parameter (See Fig. 5a, b). The major contribution to the total uncertainty in case of within-event terms is from κ and from stress drop in case of event-to-event variability (See Fig. 5a, b). The uncertainty of κ and stress parameters varies significantly with spectral period and has slow decrement for longer periods. In addition to κ, anelastic attenuation has also peaked above 0.1 s, however, its influence is similar to geometric attenuation at longer periods. Comparatively, focal depth, duration, fault plane uncertainty and random variation of hypocentral location on the fault have a very little impact on the total GMPE uncertainty. The standard deviation determined in this study is compared with the standard deviation of various GMPEs developed under the NGA-East project and stochastic for the United Kingdoms, Alps and Switzerland and given as Fig. 6. The standard deviation in case of Shahjouei and Pezeshk (2016) (SHPE-16) and Ameri et al. (2017) (AM-17) depends on magnitude and hence it is calculated at M_w 6. Standard deviation is considerable for a period less than 0.1 s in natural logarithm units and variation with period is also variable. Further, in case of Darragh et al. (2015) (Rob-1 and Rob-2), SHPE-16 and Rietbrock et al. (2013) (RB13), standard deviation is considerably high after 1 s. Peak of the Edwards and Fäh (2013), Drouet and Cotton (2015) (referred as EDF13 and DRCO15) and the present study is located between 0.05 s and 0.1 s. In the present study, between events, sigma is high at low periods, this may be due to the large variability in the stress parameters in case of variable stress GMPE.

Due to lack of recorded data, detailed validation of the newly derived ground motion prediction equation for all ranges of magnitude and distance is not possible. However, from Fig. 4, it is already seen that the recorded PGA and PSA (0.15 s) is matching well with the PGA and PSA calculated from the newly developed GMPE. Further, the response spectra of the Maharashtra Earthquake (2009) and Koyna Earthquake (1967) is compared with the predicted response spectra from GMPE and given in Fig. 7. It is seen from Fig. 7 that the predicted and derived response spectra at different hypocentral distance and magnitude is matching well and within the confidence interval, and the difference is very small for the entire period range. Minor differences at different periods may arise due to different
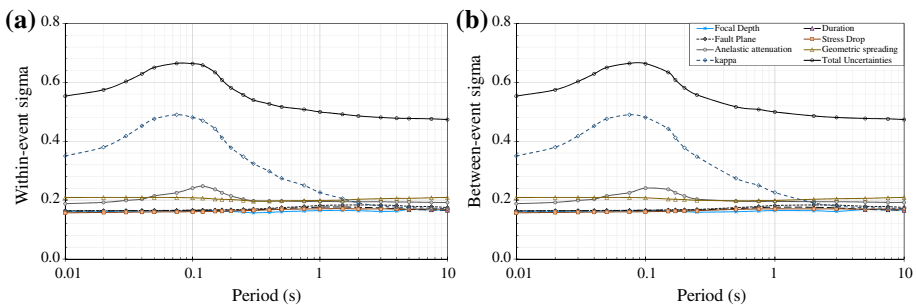

Fig. 5 **a** Within-event and **b** Between-event sigma obtained from considering seven models used in sensitivity analysis
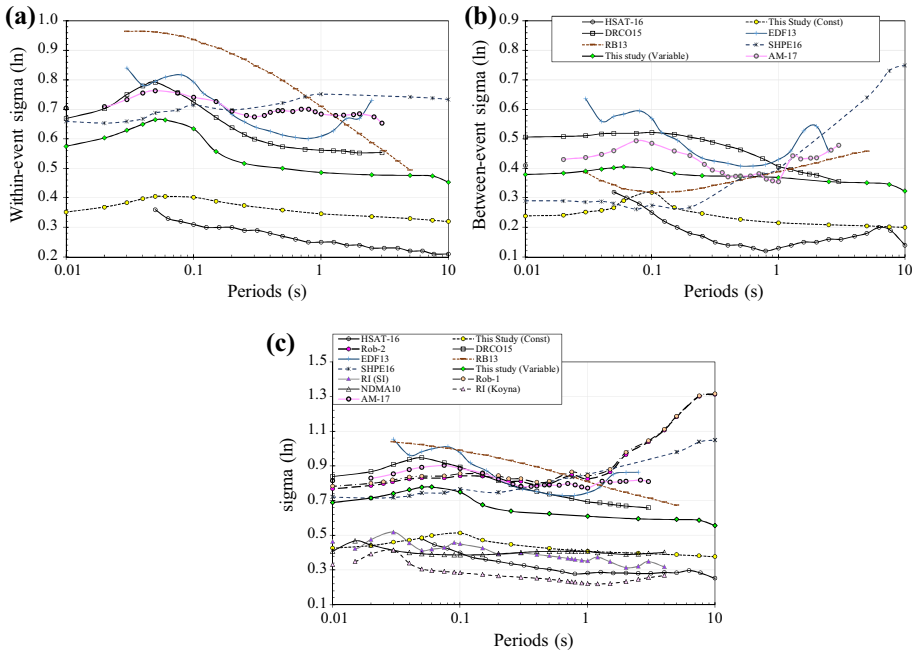
Fig. 6 Comparison of **a** Within-event; **b** Between-event and **c** Sigma standard deviations for the new Peninsular region GMPE with the NGA-East GMPES and other stochastic GMPEs. The abbreviation of the respective GMPE is given in the text
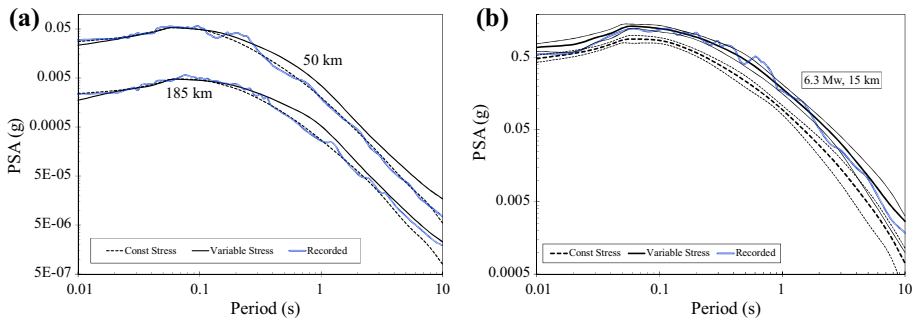

Fig. 7 Comparison of predicted and recorded response spectra **a** Maharashtra EQ (2008) and **b** Koyna EQ (1967) at different hypocentral distance

uncertainties considered while simulating the stochastic strong ground motion. Further, the error has been determined for PGA with respect to magnitude and hypocentral distance. The residual has been computed by using recorded PGA and PGA converted from MMI. For a regression model to be unbiased, the mean of the residual is to be zero and independent of the parameters in the regression model. Further for checking the bias and average scatter, average and standard deviation of the residual's errors are also calculated. Based on Fig. 8, it can be highlighted that PGA distribution of residuals with magnitude and hypocentral distance is unbiased.
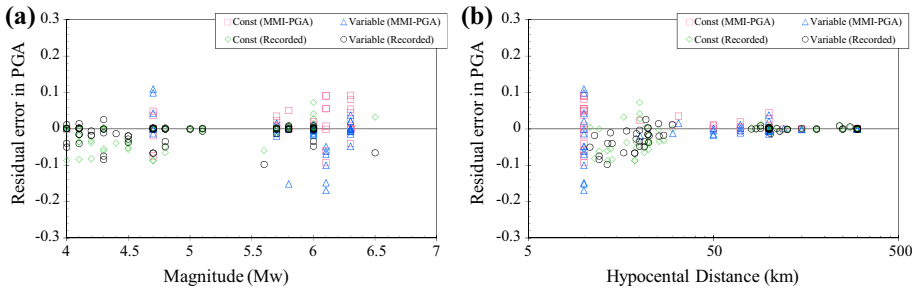
Fig. 8 Distribution of residual **a** PGA versus Magnitude; **b** PGA versus Hypocentral Distance considering both constant (const) and variable stress model derived in this study

8 Conclusion

Regional stochastic ground motion prediction equation for Peninsular India for a broad range of magnitudes (M_w 4–8) and hypocentral distances (10–500 km) is derived. The simulations are done by studying the region-specific seismological parameters and the uncertainty is propagated by random sampling of a corresponding distribution of the input parameters. It is observed that these parameters are not same for the entire Peninsular region. To capture the nonuniform seismicity, two models namely constant and variable stress were used in deriving a new GMPE. Hence, simulation is done by dividing the whole Peninsular India into five parts i.e. Eastern Dharwar Carton, Western Dharwar Carton, South Granulite Terrain, Deccan Volcanic Province and Koyna region. The functional form is derived based on the mixed effect model on the residuals calculated from recorded and simulated PGA. The simulated data is regressed using linear-mixed effect regression approach for the defined functional form for scaling the magnitude and large distance. Further, sensitivity analysis was used to find the impact of each input parameter on the total uncertainty of the ground motion prediction equation. The defined GMPE is valid for the bed rock level. PGA and SA of newly developed GMPE are matching well with the recorded data for the larger and smaller hypocentral distances.

Appendix 1

See Table 5.

Table 5 Details of instrumented and non-instrumented Earthquakes used in this study

Sl. no.	Date	Long	Lat	Mag
1	**1900-02-07**	**76.8**	**10.8**	**6.3**
2	**1938-03-14**	**75.7**	**21.5**	**6.3**
3	**1969-04-13**	**80.6**	**17.9**	**5.7**
4	**1967-12-10**	**73.7**	**17.5**	**6.5**
5	**1975-05-12**	**75.3**	**13.8**	**4.7**
6	**2000-12-12**	**76.88**	**9.71**	**4.7**
7	**1993-09-29**	**77.5**	**18.06**	**6.1**
8	2008-09-16	73.915	17.438	5
9	2009-01-04	75.33	21.58	4.1
10	2009-02-27	89.107	20.473	4.8
11	2009-04-15	82.616	6.796	4.5
12	2009-12-12	73.77	17.13	4.8
13	2009-12-12	73.45	17.12	4.3
14	2010-07-25	76.775	6.601	4
15	2011-09-19	76.56	17.92	4
16	2011-10-20	70.53	21.21	5.1
17	2012-04-14	73.601	17.25	4.4
18	2014-05-21	88.04	18.201	6
19	2014-08-24	85.8	9.072	4.1
20	2014-11-03	86.077	16.093	4.4
21	2015-12-05	71.19	18.43	4.3
22	2016-07-17	71.55	21.42	4.1
23	2017-06-03	73.576	16.669	4.3
24	2017-08-19	73.386	16.366	4.1
25	1980-09-20	73.7	17.35	4.7
26	1980-09-02	73.74	17.23	4.1
27	1993-10-08	76.4	17.93	4.3
28	1997-05-21	80.06	23.8	5.8

Earthquakes marked in bold are non-instrumental earthquakes

References

Al Norman MN, Cramer CH (2015) Empirical ground motion prediction equations for Eastern North America, PEER Report No. 2015/04, Pacific Earthquake Engineering Research Center, California, p 193

Allmann BP, Shearer PM (2009) Global variations of stress drop for moderate to large earthquakes. J Geophys Res. https://doi.org/10.1029/2008jb005821

Ameri G, Drouet S, Traversa P, Bindi D, Cotton F (2017) Toward an empirical ground motion prediction equation for France: accounting for regional differences in the source stress parameter. Bull Earthq Eng 15:4681. https://doi.org/10.1007/s10518-017-0171-1

Anbazhagan P, Kumar A, Sitharam TG (2013) Ground motion prediction equation considering combined dataset of recorded and simulated ground motions. Soil Dyn Earthq Eng 53:92–108

Anbazhagan P, Bajaj K, Moustafa SSR, Nassir SNA (2015) Maximum magnitude estimation considering the regional rupture character. J Seismol 19(3):695–719

Anbazhagan P, Sreenivas M, Bajaj K, Moustafa SS, Al-Arifi NSN (2016) Selection of ground motion prediction equations for seismic hazard analysis of Peninsular India. J Earthq Eng 20:699–737

Anbazhagan P, Sheikh NMM, Bajaj K, Moustafa SS, Al-Arifi NSN (2017) Empirical models for the prediction of ground motion duration for intraplate earthquakes. J Seismol 21:1001–1021

Bajaj K, Anbazhagan P (2018a). Regional stochastic GMPE for active region with limited strong motion data: application to the Himalayan region. Soil Dynamics and Earthquake Engineering (under review)

Bajaj K, Anbazhagan P (2018b) A comparison of different functional form and modification of NGA-West 2 ground-motion prediction equation for the Himalayan region. J Seismol 22(1):161–185

Bates DM, Maechler M, Bolker B (2013). Lme4: linear mixed-effect models using S4 classes R Manual, https://cran.r-project.org/web/packages/lme4/index.html. Accessed Nov 2017

Baumbach M, Grosser H, Schmidt HG, Paulat A, Rietbrock A, Ramakrishna Rao CV, Solomon Raju E, Sarkar D, Mohan I (1994) Study of foreshocks and aftershocks of the intraplate Latur earthquake of September 30, 1993, India, in H. K. Gupta (editor). Latur Earthq Geol Soc India Mem 35:33–63

Blaser L, Kruger F, Ohrnberger M, Scherbaum F (2010) Scaling relation of earthquake source parameter estimates with special focus on Subduction environment. Bull Seismol Soc Am 100:2914–2926

Boore DM (2003) Simulation of ground motion using the stochastic method. Pure Appl Geophys 160:635–676

Boore DM (2009) Comparing stochastic point-source and finite-source ground motion simulations: SMSIM and EXSIM. Bull Seismol Soc Am 99:3202–3216

Darragh RB, Abrahamson NA, Silva WJ, Gregor N (2015) Development of hard rock ground motion models for region 2 of Central and Eastern North America, PEER Report No. 2015/04, Pacific Earthquake Engineering Research Center, California, p 51

Drouet S, Cotton F (2015) Regional stochastic GMPEs in low-seismicity areas: scaling and aleatory variability analysis-application to the French Alps. Bull Seismol Soc Am 105:1883–1902

Edwards B, Fäh D (2013) A stochastic ground-motion model for Switzerland. Bull Seismol Soc Am 103:78–98

Frankel A, Wennerberg L (1987) Energy-flux model of the seismic coda: separation of scattering and intrinsic attenuation. Bull Seismol Soc Am 77:1223–1251

Graizer V (2015) Ground-motion prediction equations for the Central and Eastern United States. PEER Report No. 2015/04, Pacific Earthquake Engineering Research Center, California, p 213

Gupta HK (2006) Stable continental regions are more vulnerable to earthquakes than once thought. J Ind Geophys Union 10(1):59–61

Gupta SC, Kumar A (2002) Seismic wave attenuation characteristics of three Indian regions: a comparative study. Curr Sci 82:407–413

Gupta ID, Rambabu V (1993) Source parameters of some significant earthquakes near Koyna Dam, India. PAGEOPH 140(3):403–413

Ide S, Beroza GC, Prejean SG, Ellsworth WL (2003) Apparent break in earthquake 550 scaling due to path and site effects on deep borehole recordings Geophys. Res Lett 108:2271

Iyengar RN, Raghu Kanth STG (2004) Attenuation of strong ground motion in Peninsular Inida. Seismol Res Lett 75(4):530–540

John B, Rajendran CP (2008) Geomorphic indicators of neotectonism from the Precambrian terrain of Peninsular India: a case study from the Bharathapuzha Basin, Kerala. J Geol Soc India 71:827–840

Kumar CHP, Sarma CSP, Shekar M, Chadha RK (2007) Attenuation studies based on local earthquake Coda waves in the southern Indian peninsular shield. Nat Hazards 40:527–536

Meert JG, Pandit MK, Pradhan VR, Jonathan B, Sirianni R, Stroud M, Newstead B, Gifford J (2010) Precambrian crustal evolution of Peninsular India: a 3.0-billion-year odyssey. J Asian Earth Sci 39:483–515

Motazedian D, Atkinson GM (2005) Stochastic finite-fault modeling based on a dynamic corner frequency. Bull Seismol Soc Am 95:995–1010

Murthy KSR, Chaubey AK, Radhakrishna M (2011) Guest editorial for the special issue. Tectonics of Bay of Bengal and Arabian Sea with special emphasis on coastal and marine geohazards. Nat Hazards 57:1–5

Nath SK, Thingbaijam KKS (2012) Peak ground motion predictions in India: an appraisal for rock sites. J. Seismol. 15(2):295–315

Pezeshk S, Zandieh A, Campbell KW, Tavakoli B (2015). Ground-motion equations for CENA using the hybrid empirical method in conjunction with NGA-West 2 empirical ground-motion models, PEER Report No. 2015/04, Pacific Earthquake Engineering Research Center, California, p 119

Pezeshk S, Zandieh A, Campbell KW, Tavakoli B (2018) Ground-motion prediction equations for Central and Eastern North America using the hybrid empirical method and NGA-West2 empirical ground-motion models. Seismol Soc Am, Bull. https://doi.org/10.1785/0120170179

RaghuKanth STG, Iyengar RN (2007) Estimation of seismic spectral acceleration in Peninsular India. J Earth Syst Sci 116(3):199–214

Ramasamy SM (2006) Remote sensing and active tectonics of South India. Int J Remote Sens 27(20):4397–4431

Rao BR (2000) Historical seismicity deformation rates in the Indian Peninsular Shield. J Seismol 4:247–258

Rastogi BK (1992) Seismotectonics inferred from earthquakes and earthquake sequences in India during the 1980s. Curr Sci 62:101–108

Rietbrock A, Strasser FO, Edwards B (2013) A stochastic earthquake ground-motion prediction model for the United Kingdom. Bull Seismol Soc Am 103:57–77

Shahjouei A, Pezeshk S (2016) Alternative hybrid empirical ground-motion model for Central and Eastern North America using hybrid simulations and NGA-West2 Models. Bull Seismol Soc Am 106:734–754

Singh SK, Ordaz M, Dattatrayam RS, Gupta HK (1999) A spectral analysis of the May 21, 1997, Jabalpur, India Earthquake ($M_w = 5.8$) and estimation of ground motion from future earthquakes in the Indian Shield Region. Bull Seismol Soc Am 89:1620–1630

Singh C, Basha SK, Shekar M, Chadha RK (2012) Spatial variation of coda wave attenuation in the Southern Indian Shield and its implications. Geol Acta 10(3):309–318

Sivaram K, Utpal S, Kanna N, Kumar D (2017) Attenuation characteristics of high frequency seismic waves in Southern India. Pure Appl Geophys 174:2523–2545

Skarlatoudis AA (2017) Applicability of ground-motion prediction equations to a Greek within-slab earthquake dataset. Bull Earthq Eng 15:3987. https://doi.org/10.1007/s10518-017-0140-8

Stafford PJ (2014) Crossed and nested mixed-effects approaches for enhanced model development and removal of the ergodic assumption in empirical ground-motion models. Bull Seismol Soc Am 104:702–719

Subbarao KV, Hooper PR (1988). Reconnaissance map of the Deccan basalt group in Western Ghats, India, in Deccan Flood Basalts, edited by K. V. Subbarao, Memories Geological Society of India, No. 10

Yadav A, Shashidhar D, Mallika K, Purnachandra NR, Rohilla S, Satyanarayana HVS, Srinagesh D, Gupta H (2013) Source parameters of earthquakes in the reservoir-triggered seismic (RTS) zone of Koyna-Warna, Western India. Nat Hazards 69:965–979